■ **Supramolecular Chemistry**

Mechanistic Insights into the Self-Assembly of an Acid-Sensitive Photoresponsive Supramolecular Polymer

Kalathil K. Kartha,[a] Naveen Kumar Allampally,[b] Shiki Yagai,[c] Rodrigo Q. Albuquerque,[a] and Gustavo Fernández*[a]

Abstract: The supramolecular polymerization of an acid-sensitive pyridyl-based ligand (L_1) bearing a photoresponsive azobenzene moiety was elucidated by mechanistic studies. Addition of trifluoroacetic acid (TFA) led to the transformation of the antiparallel H-bonded fibers of L_1 in methylcyclohexane into superhelical braid-like fibers stabilized by H-bonding of parallel-stacked monomer units. Interestingly, L_1 dimers held together by unconventional pyridine–TFA N···H···O bridges represent the main structural elements of the assembly. UV-light irradiation caused a strain-driven disassembly and subsequent aggregate reconstruction, which ultimately led to short fibers. The results allowed to understand the mechanism of mutual influence of acid and light stimuli on supramolecular polymerization processes, thus opening up new possibilities to design advanced stimuli-triggered supramolecular systems.

Introduction

Supramolecular functional materials derived from discrete π-systems have attracted considerable attention during the past few decades, primarily due to their promising optoelectronic[1] and biomedical applications.[2] These smart materials held together through multiple noncovalent interactions have the advantage of reversible changes in the physical properties as a response towards various stimuli, including temperature,[3] light,[4] mechanical stress,[5] ultrasounds,[6] metal ions,[7] redox reactions[8] and pH.[9] Successful candidates are often used as sensors,[10] switches,[11] as well as for drug delivery.[12] In particular, light-responsive organogelators derived from azobenzenes,[13] spiropyrans[14] and diaryethenes[15] have been widely exploited in the field of self-assembled materials due to their potential application in the area of storage and secret documentation.[16] The *trans*-to-*cis* photoisomerization of the azo-benzene groups has been used to reversibly control gel–sol transitions, which eventually has produced smart photoresponsive materials.[17] In addition to the significant development in the field of light-responsive organogelators, more advanced multistimuli-responsive gelators based on azobenzene have been recently reported.[18, 19] However, detailed mechanistic investigations of their triggered self-assembly remain scarce.

Recently, we have reported the reciprocal impact of light irradiation and metal coordination on the hierarchical self-assembly of an azo-containing pyridyl ligand (molecule L_1 in Scheme 1).[20] The ability of the pyridyl ligand to bind metal ions, such as Pd^{II}, was investigated in terms of its influence on the self-assembly and photoresponsive behavior. However, the pyridyl group can be also exploited as an acid-sensitive unit in order to effectively tune self-assembly processes in solution. Here, we examine the interplay of acid and light irradiation in the supramolecular polymerization of L_1 (Scheme 1). Interestingly, we found that addition of acid to the fiber-like assemblies of L_1 enhances the aggregation and leads to the formation of unique superhelical structures through stacking of acid-bridged L_1-dimers. Furthermore, we found that the light irradiation could cause disassembly of the superhelical fibers and their reconstruction into thin fibers through a different pathway associated with a rapid *cis*–*trans* isomerization under isothermal conditions.

Results and Discussion

Self-assembly and gelation of L_1

Gelation studies of L_1 were performed in different organic solvents and the majority of them were immobilized upon addition of L_1 in excess. Pictures of all gels under daylight are shown in Figure S1 (Supporting Information), whereas Table S1

[a] Dr. K. K. Kartha, Dr. R. Q. Albuquerque, Prof. Dr. G. Fernández
Organisch-Chemisches Institut, Westfälische Wilhelms-Universität Münster
Corrensstraße 40, 48149 Münster (Germany)
E-mail: fernandg@uni-muenster.de

[b] Dr. N. K. Allampally
Institut für Organische Chemie, Universität Würzburg
am Hubland, 97074 Würzburg (Germany)

[c] Prof. Dr. S. Yagai
Department of Applied Chemistry and Biotechnology
Graduate School of Engineering, Chiba University
1-33-Yayoi-cho, Inage-Ku, Chiba 263-8522 (Japan)
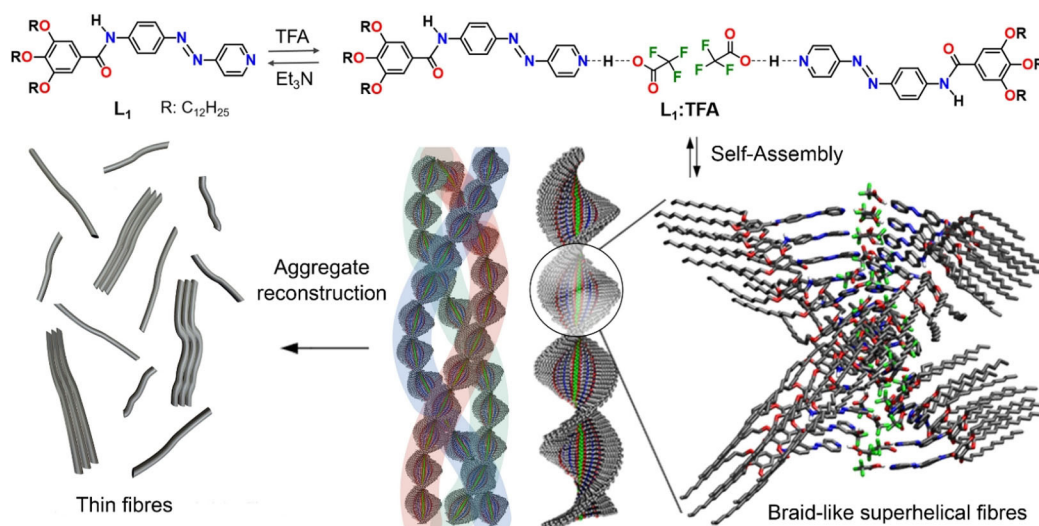
Scheme 1. Molecular structure of **L₁** and schematic representation of its self-assembly behavior as a response towards acid and UV light. The superhelical fibers (right, bottom) were optimized through dispersion-corrected PM6 semiempirical calculations (nonpolar hydrogens were omitted for clarity).

provides information about their critical gelation concentration (CGC) values in various solvents. A minimum CGC of 2.31 mg mL⁻¹ in isooctane and a maximum of 16.36 mg mL⁻¹ in *n*-butanol were marked as the lower and upper benchmarks. From these values, one can clearly notice that hydrophobic solvents readily and most effectively gelate **L₁** (Table S1, Supporting Information). The CGC values decrease upon increasing the *n*-hydrocarbon chain length of the solvents, confirming the role of hydrophobic interactions.

Interestingly, gels in toluene cannot be obtained even at very high concentrations, which could be explained in terms of attenuated aromatic interactions. Moreover, *n*-alcohols can also induce gelation, although with higher CGC values compared to analogous *n*-hydrocarbons. These results suggest a strong contribution of H-bonding to the gelation process in hydrocarbon solvents, whereas in *n*-alcohols these interactions are weakened. On this basis, we can conclude that H-bonding as well as aromatic and hydrophobic interactions are the primary forces responsible for gel formation. The morphology of the xerogels formed in selected solvents [isooctane and methylcyclohexane (MCH), see Figure 1] was examined by atomic force microscopy (AFM) on highly oriented pyrolytic graphite (HOPG). For both samples, densely packed networks of entan-
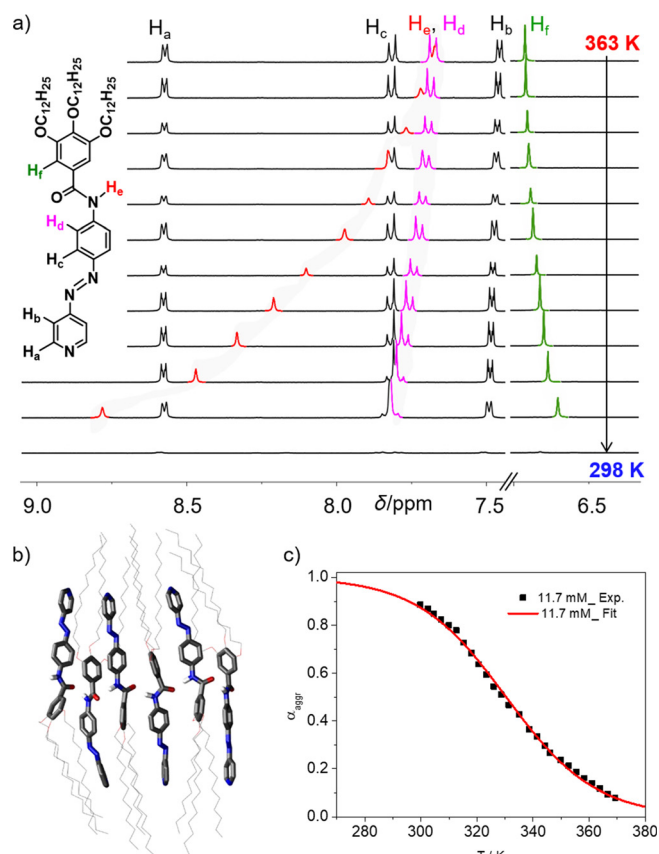
gled fibers could be observed. Additionally, scanning electron microscopy (SEM) studies on glass substrate confirmed the fibrillar morphology of the xerogels (Figure S2, Supporting Information).
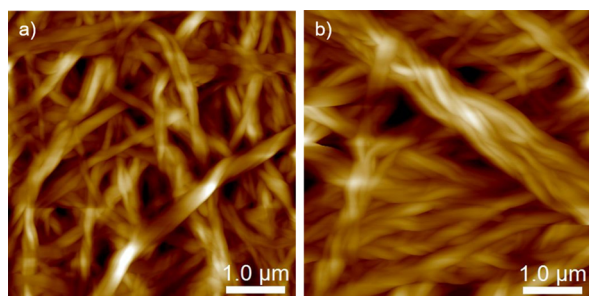
Considering that MCH yielded stable gels and is commonly used for aggregation studies, we selected this solvent as ideal medium for gelation as well as pH- and light-responsive studies. Figure 2a shows the variable-temperature (VT) ¹H NMR experiments at 11.7 mM obtained by cooling a solution of **L₁** in MCH-d₁₄ from a molecularly dissolved state (363 K) to a gel state (298 K) in steps of 2.5 K. The spectra show noticeable chemical shifts upon decreasing temperature. For instance, although the signals of the amide protons H_e and those of protons H_d are downfield shifted, the proton signals of the outer aromatic rings (H_f) undergo a shielding effect upon decreasing temperature (Figure 2a). Alternatively, pyridyl protons H_a and H_b and protons H_c from the central aromatic rings are barely sensitive to temperature (Figure 2a). In particular, the strong downfield shift (≈ 7.55 to 8.95 ppm) observed for the amide protons (H_e) upon decreasing temperature (Figure 2a,b) confirms the active involvement of H-bonding in the aggregation process. A comparably smaller downfield shift observed also for H_d can be due the close proximity of -C=O group. In addition, the observed shifts for protons H_{a-d} are in perfect agreement with the behavior of **L₁** in more diluted solutions (10^{-4} M) and indicate an anti-parallel organization of the molecules of **L₁** in the MCH gel (Figure 2b).[20] The changes in the NMR chemical shifts of some of these protons, that is, H_c and H_d, were monitored upon temperature variation to determine the aggregation mechanism and the corresponding thermodynamic parameters.

Plotting the fraction of aggregated species (α_{agg}) against temperature afforded a sigmoidal curve, suggesting that the self-assembly of **L₁** occurs in a non-cooperative manner. Application of the isodesmic model[21] affords good fits (Figure 2c) whereas the corresponding Van't Hoff fit shows clear linearity


Figure 1. Surface morphology of xerogels of **L₁** in isooctane (a) and MCH (b) visualized by AFM on HOPG.

a)

Figure 2. a) VT ^{1}H NMR of **L$_1$** at 11.7 mM in MCH-d_{14}, b) antiparallel **L$_1$** hexamer optimized by dispersion-corrected PM6 calculations. c) plot of α_{agg} vs. T and fit to the isodesmic model (α_{agg} was calculated by monitoring the shifts of H$_d$).

(Figure S3, Supporting Information), demonstrating the suitability of the aggregation model to our data. The self-assembly process is enthalpy-driven (-63.62 kJ mol^{-1}) with an association constant (K) of 585 M^{-1}. The melting temperature (T_m) for the assembly process is 330 K (Table S2, Supporting Information). This relatively low K value also matches well with the previously observed lack of aggregation of **L$_1$** in more diluted MCH solutions (0.1 mM) at room temperature.

Influence of addition of acid on the self-assembly of L$_1$

The presence of a basic pyridine moiety in **L$_1$** endows our system with stimuli-responsiveness towards acids. Initially, a gel (11.7 mM) in MCH was prepared and its sol-to-gel reversibility was tested for several cycles (Figure 3). Addition of 2 μL of
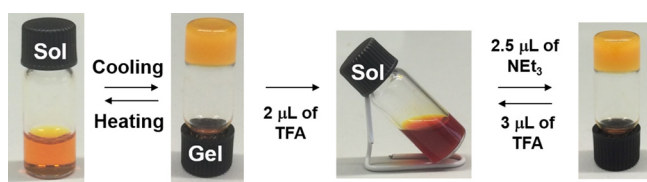
Figure 3. Pictures showing the reversible sol-to-gel transformation of **L$_1$** in MCH (11.7 mM) on heating and cooling and addition of TFA and Et$_3$N.

trifluoroacetic acid (TFA, 1 equiv) leads to the transformation of the orange-colored opaque gel into a clear red-colored solution only few seconds after TFA addition. These findings strongly suggest the protonation of the pyridine groups of **L$_1$** upon TFA addition and the subsequent cleavage of the gel network, most likely as a result of electrostatic repulsion of the positive charges and decrease in solubility of the monomer units. Notably, the gel can be regenerated within 5 minutes after addition of 1 equivalent of triethylamine (Et$_3$N) (Figure 3) due to the deprotonation of the pyridyl groups. The reversibility of the sol-to-gel transformation could be reproduced for various cycles of acid/base addition without signs of decomposition.

To gain closer insights into the impact of acid addition on the aggregation behavior, an MCH solution of **L$_1$** under more diluted conditions (5×10^{-4} M) was titrated against TFA and monitored by UV/Vis absorption spectroscopy. A significant redshift from 362 to 390 nm with broadening in the absorption spectrum was observed upon addition of 0.1 to 1 equivalents of TFA to the **L$_1$** solution, which can be assigned to the protonation of the pyridyl group of **L$_1$**. No detectable emission was observed for **L$_1$** before or after addition of TFA. To rule out a partial aggregation of **L$_1$** prior to TFA addition (**L$_1$** was previously observed to aggregate slowly over time at 5×10^{-4} M in MCH), we titrated **L$_1$** with TFA in a good solvent (chloroform), in which both species are soluble and no aggregation of **L$_1$** takes place. Similarly to MCH, the formation of a red-colored solution upon addition of 1 equiv TFA supports the protonation of the pyridyl group of molecularly dissolved **L$_1$** (Figure 4a,
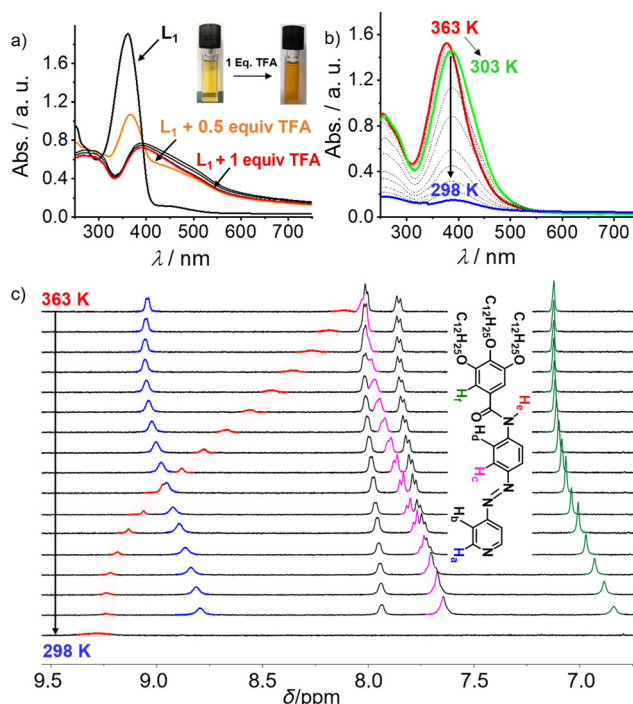


Figure 4. a) Absorption changes of **L$_1$** (5×10^{-4} M) in CHCl$_3$ upon addition of increasing amounts of TFA (inset: photographs showing the color change upon addition of 1 equiv of TFA). b) VT UV/Vis (0.5 mM, MCH) and c) VT ^{1}H NMR experiments of **L$_1$**:TFA complex between 363 and 298 K (0.5 mM, MCH-d_{14}).

inset). Subsequently, the solvent (chloroform) was removed to obtain the **L₁:TFA** species as a red powder. Finally, to examine the impact of TFA addition on the self-assembly, the powder was redissolved in MCH to induce aggregation. This equimolar mixture of **L₁** and TFA in MCH was subsequently heated to 363 K to ensure the formation of a monomer state and subjected to a VT UV/Vis experiment using a cooling rate of 1 K min⁻¹ (Figure 4 b). Upon cooling down to 303 K, a 10 nm redshift in the absorption spectrum was observed (377 to 387 nm). This behavior can be ascribed to a *J*-type aggregate formation, which has been previously observed for related acid-sensitive pyridine-based two-component systems.[22] Additionally, further cooling to 298 K induces the formation of higher order aggregates in solution, which is also visible with the naked eye and evidenced by a significant decrease of the absorption band (Figure 4 b).

VT ¹H NMR measurements under identical conditions showed a significant deshielding (8.11 to 9.29 ppm) of the amide N–H protons on cooling, indicative of strong H-bonding (Figure 4 c). Alternatively, all other aromatic signals were shielded upon cooling due to their active involvement in π–π stacking. These shifts differ significantly from those of the neutral ligand **L₁**, which anticipate a distinct molecular arrangement in the self-assembled structure. Although for the neutral ligand the pyridyl protons (Hₐ and H_b) experience negligible shifts upon cooling, these protons shift upfield for the protonated form (see comparison in Figures 2 a and 4 c). This distinct pattern suggests a parallel stacking of the protonated monomer units within the aggregate, in contrast to the antiparallel arrangement[23] observed for the neutral form. To determine the aggregation mechanism and the corresponding thermodynamic parameters of **L₁:TFA** in MCH, the changes in the chemical shift of H_c were monitored upon temperature variation. The plot of α_{agg} against temperature shows a sigmoidal curve that can be fitted to the isodesmic model (Figure S4, Supporting Information). The self-assembly process is enthalpy driven ($\Delta H = -89.24$ kJ mol⁻¹) with an association constant (*K*) of 1171 M⁻¹. This calculated *K* value is approximately twice larger than that of the neutral ligand **L₁**. The T_m for the self-assembly process is 324 K (Table S2, Supporting Information). In accordance with UV/Vis absorption spectroscopy studies, cooling the **L₁:TFA** mixture below 303 K in VT NMR led to the formation of higher order aggregates as evident from the broadening and disappearance of NMR signals (Figure 4 c, bottom spectrum), most likely due to the activation of secondary interactions. The rearrangement from an anti-parallel organization of **L₁** to a parallel organization of **L₁:TFA** in MCH may be caused by the presence of an electrostatic environment created on the pyridyl nitrogen and decreased solubility of the polar protonated species in the nonpolar (MCH) medium.

To examine the morphology of **L₁:TFA** (1:1) complex in MCH, AFM imaging has been performed by spin coating a 5×10^{-4} M aggregate solution onto HOPG. Interestingly, micrometer long and entangled helical fibers with 20–40 nm height and 200–400 nm width were observed, as shown in Figure 5. Notably, these fibers do not lead to gelation but rather to the formation of red precipitates when the concentration of the protonated
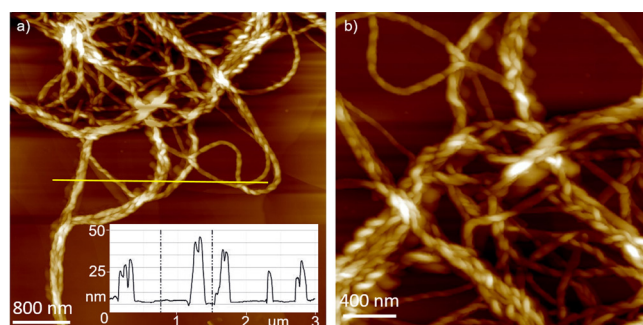

Figure 5. AFM images of **L₁:TFA** (1:1; 5×10^{-4} M) in MCH prepared by spin-coating onto HOPG (inset: cross-section analysis along the yellow line).

species is increased above 5×10^{-4} M. These results contrast with those previously observed for the neutral ligand **L₁**, in which a strong gelation ability was found. Thus, it can be concluded that protonation of the pyridyl group of **L₁** does not cause the disassembly of the fibers into the free monomers, as commonly observed for various pH-responsive organogelators,[9b,e] but rather to a new molecular rearrangement leading to distinct aggregate morphology. No circular dichroism (CD) signals could be observed upon cooling from 363 to 283 K ($c = 5 \times 10^{-4}$ M; Figure S5, Supporting Information), indicating a non-preferred (racemic mixture of P and M helices) organization of the achiral **L₁:TFA** in MCH.

The proposed acid-driven parallel molecular arrangement of the **L₁:TFA** complex was investigated and optimized using the dispersion-corrected PM6 semiempirical method (Scheme 1, bottom right; Figure 6 and Figure S6 in the Supporting Information). The calculations suggest that a **L₁:TFA** dimer (**L₁:TFA:TFA:L₁**) represents the main structural element of the helical supramolecular structure (see also Movie S1 in the Supporting Information). Electric dipole moments are optimally cancelled inside each dimer, the carbonyls of the amide groups being antiparallel to each other. TFA units are also oriented antiparallel within each dimer. One proton is shared between the pyridine nitrogen and the carboxylic oxygen of TFA, giving rise to an N···H···O bridge, which enables dimer formation (see Figures 6 and Figure S6 in the Supporting Information). In addition, aromatic interactions and amide H-bonding between neighboring dimers further stabilize the helical structure, which is in accordance with the VT UV/Vis and VT NMR results. Van der Waals interactions between alkyl chains are also important to stabilize the supramolecule, as shown in Scheme 1.

Photoresponsive behavior of L₁:TFA assembly

Irradiation of the **L₁:TFA** helical aggregates in MCH with a UV LED for 30 min led to the transformation of the initially turbid solution to a clear solution without any color change (Figure 7 a, inset). The absence of any significant hypsochromic shifts demonstrates that the **L₁:TFA** pairs remain stable upon UV irradiation without disassembly into the free ligand **L₁**. However, the fact that marked hyperchromic UV/Vis absorption changes are observed upon UV irradiation (Figure 7 a) are in
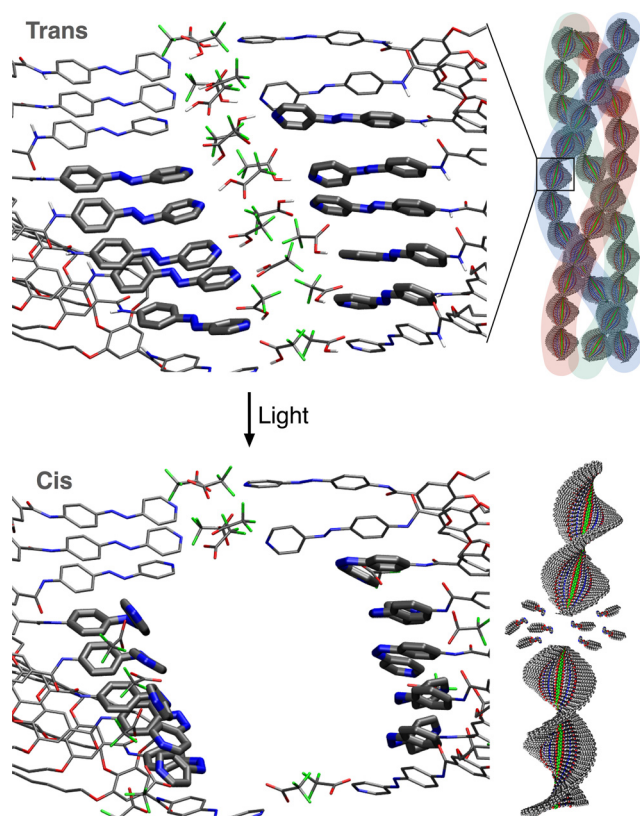
Figure 6. Dispersion-corrected PM6 optimized helix of the **L₁:TFA** dimer before (top) and after (bottom) UV-light irradiation, with the highlighted azobenzene groups in the *trans* (top) or *cis* (bottom) conformation.

Figure 7. Time-dependent a) UV/Vis absorption (pink: 0 min; blue: 180 min after UV irradiation for 30 min at 298 K; inset showing corresponding photographs) and b) ¹H NMR changes of **L₁:TFA** (1:1, 5×10^{-4} M) in MCH-d_{14}: before (i) and 0 min (ii), 2 h (iii), and 12 h (iv) after UV irradiation for 30 min at 298 K. c,d) AFM images of **L₁:TFA** (1:1; 5×10^{-4} M) in MCH on HOPG after incubating the irradiated sample at 298 K for 12 h (inset of panel d: cross-section analysis along the yellow line).

accordance with a possible strain-driven disassembly.[24] Further keeping the solution at 298 K for 3 hours in the dark showed a decrease in absorbance without negligible shifts, indicating a reconstruction of the aggregates. If the solution was kept at 298 K for longer than 3 hours, slow precipitation occurred, possibly due to the formation of higher order assemblies. ¹H NMR measurements were performed to monitor the reconstruction as shown in Figure 7 b. As expected, the initial NMR spectrum of the higher order helical assemblies of **L₁:TFA** is poorly defined (Figure 7 b, top). However, the appearance of sharp signals of the *trans*-azobenzene moieties right after irradiation of the **L₁:TFA** aggregates for 30 minutes (denoted as $t=0$) is in accordance with UV changes and suggests a light-induced disassembly process. This observation can be ascribed to the *trans*-to-*cis* photoisomerization of the azobenzene and subsequent rapid thermal *cis*-to-*trans* isomerization.[25] Prolonged incubation at 298 K for approximately 12 hours under dark conditions after photoirradiation causes the complete disappearance of the NMR signals, most likely due to the formation of a new assembly that is large in size. AFM measurements on HOPG further supported the reconstruction of assemblies. The images reveal short fibers with a length of approximately 500 nm and height of 1–2 nm, as shown in Figure 7. When the solution was incubated for 12 hours under dark at 298 K followed by spin-coating on a HOPG surface, only bundling of thin and short fibers were observed (Figure 7 d). Such a transformation of long entangled network of fibers into short and

thin fibers after photoirradiation under isothermal conditions indicates that the self-assembly of **L₁:TFA** can proceed through a different pathway, as also recently proposed for an azobenzene amphiphile in a liquid crystalline state.[25] The absence of any shifts in the UV/Vis spectra of the thin fibers compared to the superhelices (Figure S7, Supporting Information) suggests that the molecular packing is nearly unaffected upon light irradiation and subsequent photo-reconstruction. Only a weak additional shoulder band around 525 nm is observed for the thin fibers, which might suggest slight differences in translational and/or rotational offsets of the molecules for the two assemblies.

Conclusion

In summary, we have elucidated the effect of acid addition on the self-assembly pathways of a photoresponsive ligand (**L₁**). In the absence of acid and light, **L₁** self-assembles in MCH into micrometer-sized twisted fibers and gels through strong amide H-bonding and aromatic interactions of antiparallel-arranged monomer units. Unlike multiple examples of previously reported acid-sensitive gelators, addition of TFA does not simply lead to a nanostructure disassembly, but rather to the molecular reorganization through a different pathway into superhelical braid-like fibers. A combination of NMR and UV/Vis absorption spectroscopies as well as AFM and theoretical calculations suggested that **L₁** dimers held together by two pyridine–TFA N···H···O bridges are the main structural elements of the supramolecular helical structures. A preferred parallel stacking of these **L₁** dimers supported by amide H-bonds and van der Waals interactions involving the alkyl chains enables the forma-

tion of superstructures, an arrangement that also serves to shield the polar groups from the nonpolar environment. The orientation of the TFA counteranions in an antiparallel fashion further stabilizes the helical assembly by cancelling the electric dipole moments. Ultimately, the photoresponsive behavior of the **L₁:TFA** species was also examined. Notably, a plausible reconstruction of the initial superhelical fibers into short fibers occurs through a strain-driven disassembly and subsequent reconstruction. Overall, our findings may contribute to an increased understanding of the relationship between acid and light and their mutual impact on supramolecular polymerization processes.

Experimental Section

Synthetic procedures, materials and methods: The synthesis of **L₁** has been previously reported.[20] The xerogel was prepared by heating the gel to sol and a few mL of sol was quickly dropped on to HOPG substrate. On leaving at room temperature, the gel was formed and the solvent was evaporated under vacuum before measurement. **L₁:TFA** dimer was prepared by dissolving equimolar amounts of **L₁** and **TFA** in CHCl₃ and subsequent evaporation of solvent under ambient conditions. The sample was dried under vacuum before using it for further experiments.

Acknowledgements

Conflict of interest

The authors declare no conflict of interest.

[1] a) S. S. Babu, S. Prasanthkumar, A. Ajayaghosh, *Angew. Chem. Int. Ed.* **2012**, *51*, 1766–1776; *Angew. Chem.* **2012**, *124*, 1800–1810; b) E. Busseron, Y. Ruff, E. Moulin, N. Giuseppone, *Nanoscale* **2013**, *5*, 7098–7140; c) A. Das, S. Ghosh, *Angew. Chem. Int. Ed.* **2014**, *53*, 2038–2054; *Angew. Chem.* **2014**, *126*, 2068–2084; d) S. S. Babu, V. K. Praveen, A. Ajayaghosh, *Chem. Rev.* **2014**, *114*, 1973–2129; e) *Supramolecular Materials for Opto-Electronics* (Ed.: N. Koch), Royal Society of Chemistry, Cambridge, **2015**; f) A. Jain, S. J. George, *Mater. Today* **2015**, *18*, 206–214.

[2] a) R. Dong, Y. Zhou, X. Huang, X. Zhu, Y. Lu, J. Shen, *Adv. Mater.* **2015**, *27*, 498–526; b) X. Du, J. Zhou, J. Shi, B. Xu, *Chem. Rev.* **2015**, *115*, 13165–13307; c) *Smart Materials for Tissue Engineering: Applications* (Ed.: Q. Wang), Royal Society of Chemistry, Croydon, **2017**; d) A. Sampedro, A. Ramos-Torres, C. Schwöppe, C. Mück-Lichtenfeld, I. Helmers, A. Bort, I. Diaz-Laviada Marturet, G. Fernandez, *Angew. Chem. Int. Ed.* **2018**, *57*, 17235–17239; *Angew. Chem.* **2018**, *130*, 17481–17485; e) M. Golla, S. P. Thadi, D. Perumal, S. Atchimnaidu, R. Varghese, *ChemNanoMat* **2018**, *4*, 1153–1159.

[3] a) T. F. A. De Greef, M. M. J. Smulders, M. Wolffs, A. P. H. J. Schenning, R. P. Sijbesma, E. W. Meijer, *Chem. Rev.* **2009**, *109*, 5687–5754; b) J. D. Tovar, *Acc. Chem. Res.* **2013**, *46*, 1527–1537; c) C. Kulkarni, S. Balasubra-

manian, S. J. George, *ChemPhysChem* **2013**, *14*, 661–673; d) C. Rest, R. Kandanelli, G. Fernandez, *Chem. Soc. Rev.* **2015**, *44*, 2543–2572; e) D. B. Amabilino, D. K. Smith, J. W. Steed, *Chem. Soc. Rev.* **2017**, *46*, 2404–2420; f) A. Sorrenti, J. Leira-Iglesias, A. J. Markvoort, T. F. A. de Greef, T. M. Hermans, *Chem. Soc. Rev.* **2017**, *46*, 5476–5490.

[4] a) S. Yagai, A. Kitamura, *Chem. Soc. Rev.* **2008**, *37*, 1520–1529; b) S. Mahesh, A. Gopal, R. Thirumalai, A. Ajayaghosh, *J. Am. Chem. Soc.* **2012**, *134*, 7227–7230; c) M. Endo, T. Fukui, S. H. Jung, S. Yagai, M. Takeuchi, K. Sugiyasu, *J. Am. Chem. Soc.* **2016**, *138*, 14347–14353; d) S. Yagai, M. Yamauchi, A. Kobayashi, T. Karatsu, A. Kitamura, T. Ohba, Y. Kikkawa, *J. Am. Chem. Soc.* **2012**, *134*, 18205–18208; e) B. Adhikari, Y. Yamada, M. Yamauchi, K. Wakita, X. Lin, K. Aratsu, T. Ohba, T. Karatsu, M. J. Hollamby, N. Shimizu, H. Takagi, R. Haruki, S.-i. Adachi, S. Yagai, *Nat. Commun.* **2017**, *8*, 15254.

[5] a) Z. Chi, X. Zhang, B. Xu, X. Zhou, C. Ma, Y. Zhang, S. Liu, J. Xu, *Chem. Soc. Rev.* **2012**, *41*, 3878–3896; b) S. Yagai, S. Okamura, Y. Nakano, M. Yamauchi, K. Kishikawa, T. Karatsu, A. Kitamura, A. Ueno, D. Kuzuhara, H. Yamada, T. Seki, H. Ito, *Nat. Commun.* **2014**, *5*, 4013; c) *Mechanochromic Fluorescent Materials: Phenomena, Materials and Applications* (Eds.: J. Xu, Z. Chi), Royal Society of Chemistry, Cambridge, **2014**; d) K. K. Kartha, V. S. Nair, V. K. Praveen, M. Takeuchi, A. Ajayaghosh, *J. Mater. Chem. C* **2019**, *7*, 1292–1297.

[6] a) G. Cravotto, P. Cintas, *Chem. Soc. Rev.* **2009**, *38*, 2684–2697; b) M. Malicka, A. Sandeep, F. Monti, E. Bandini, M. Gazzano, C. Ranjith, V. K. Praveen, A. Ajayaghosh, N. Armaroli, *Chem. Eur. J.* **2013**, *19*, 12991–13001; c) J. Kumar, T. Nakashima, T. Kawai, *Langmuir* **2014**, *30*, 6030–6037; d) X. Yu, L. Chen, M. Zhang, T. Yi, *Chem. Soc. Rev.* **2014**, *43*, 5346–5371; e) V. K. Pandey, M. K. Dixit, S. Manneville, C. Bucher, M. Dubey, *J. Mater. Chem. A* **2017**, *5*, 6211–6218.

[7] a) S. Shin, S. Lim, Y. Kim, T. Kim, T.-L. Choi, M. Lee, *J. Am. Chem. Soc.* **2013**, *135*, 2156–2159; b) C. G. Pappas, T. Mutasa, P. W. J. M. Frederix, S. Fleming, S. Bai, S. Debnath, S. M. Kelly, A. Gachagan, R. V. Ulijn, *Mater. Horiz.* **2015**, *2*, 198–202; c) C. A. Offiler, C. D. Jones, J. W. Steed, *Chem. Commun.* **2017**, *53*, 2024–2027.

[8] a) X. Yang, G. Zhang, D. Zhang, D. Zhu, *Langmuir* **2010**, *26*, 11720–11725; b) X.-J. Wang, L.-B. Xing, W.-N. Cao, X.-B. Li, B. Chen, C.-H. Tung, L.-Z. Wu, *Langmuir* **2011**, *27*, 774–781; c) R. Afrasiabi, H.-B. Kraatz, *Chem. Eur. J.* **2015**, *21*, 7695–7704; d) T. He, K. Li, N. Wang, Y.-X. Liao, X. Wang, X.-Q. Yu, *Soft Matter* **2014**, *10*, 3755–3761.

[9] a) Y. Li, K. M.-C. Wong, A. Y.-Y. Tam, L. Wu, V. W.-W. Yam, *Chem. Eur. J.* **2010**, *16*, 8690–8698; b) M. D. Segarra-Maset, V. J. Nebot, J. F. Miravet, B. Escuder, *Chem. Soc. Rev.* **2013**, *42*, 7086–7098; c) S. K. Albert, H. V. P. Thelu, M. Golla, N. Krishnan, R. Varghese, *Chem. Eur. J.* **2017**, *23*, 8348–8352; d) Y. Kim, H. Li, Y. He, X. Chen, X. Ma, M. Lee, *Nat. Nanotechnol.* **2017**, *12*, 551–558; e) X. Liu, H. Li, Y. Kim, M. Lee, *Chem. Commun.* **2018**, *54*, 3102–3105.

[10] a) L. Zang, Y. Che, J. S. Moore, *Acc. Chem. Res.* **2008**, *41*, 1596–1608; b) K. K. Kartha, A. Sandeep, V. K. Praveen, A. Ajayaghosh, *Chem. Rec.* **2015**, *15*, 252–265; c) P. Xue, J. Ding, Y. Shen, H. Gao, J. Zhao, J. Sun, R. Lu, *J. Mater. Chem. C* **2017**, *5*, 11532–11541; d) P. Anees, V. K. Praveen, K. K. Kartha, A. Ajayaghosh in *Comprehensive Supramolecular Chemistry II* (Ed.: C. Raston), Elsevier, Amsterdam, **2017**, pp. 297–320.

[11] a) X. Wang, C. Gu, H. Zheng, Y.-M. Zhang, S. X.-A. Zhang, *Chem. Asian J.* **2018**, *13*, 1206–1212; b) R. Rodríguez, E. Quiñoá, R. Riguera, F. Freire, *Chem. Mater.* **2018**, *30*, 2493–2497.

[12] a) A. R. Hirst, B. Escuder, J. F. Miravet, D. K. Smith, *Angew. Chem. Int. Ed.* **2008**, *47*, 8002–8018; *Angew. Chem.* **2008**, *120*, 8122–8139; b) V. M. P. Vieira, L. L. Hay, D. K. Smith, *Chem. Sci.* **2017**, *8*, 6981–6990; c) K. Sarkar, P. Dastidar, *Langmuir* **2018**, *34*, 685–692.

[13] a) S. Yagai, T. Nakajima, K. Kishikawa, S. Kohmoto, T. Karatsu, A. Kitamura, *J. Am. Chem. Soc.* **2005**, *127*, 11134–11139; b) S. J. Asshoff, F. Lancia, S. Iamsaard, B. Matt, T. Kudernac, S. P. Fletcher, N. Katsonis, *Angew. Chem. Int. Ed.* **2017**, *56*, 3261–3265; *Angew. Chem.* **2017**, *129*, 3309–3313; c) S. Engel, N. Möller, B. J. Ravoo, *Chem. Eur. J.* **2018**, *24*, 4741–4748.

[14] a) Z. Qiu, H. Yu, J. Li, Y. Wang, Y. Zhang, *Chem. Commun.* **2009**, 3342–3344; b) Q. Chen, D. Zhang, G. Zhang, X. Yang, Y. Feng, Q. Fan, D. Zhu, *Adv. Funct. Mater.* **2010**, *20*, 3244–3251; c) C. Liu, D. Yang, Q. Jin, L. Zhang, M. Liu, *Adv. Mater.* **2016**, *28*, 1644–1649.

[15] a) T. Kudernac, S. J. van der Molen, B. J. van Wees, B. L. Feringa, *Chem. Commun.* **2006**, 3597–3599; b) B. Roubinet, M. Weber, H. Shojaei, M.

Bates, M. L. Bossi, V. N. Belov, M. Irie, S. W. Hell, *J. Am. Chem. Soc.* **2017**, *139*, 6611 – 6620; c) D. Kim, J. E. Kwon, S. Y. Park, *Adv. Funct. Mater.* **2018**, *28*, 1706213.

[16] a) R. Thirumalai, R. D. Mukhopadhyay, V. K. Praveen, A. Ajayaghosh, *Sci. Rep.* **2015**, *5*, 9842; b) H. Sun, S. Liu, W. Lin, K. Y. Zhang, W. Lv, X. Huang, F. Huo, H. Yang, G. Jenkins, Q. Zhao, W. Huang, *Nat. Commun.* **2014**, *5*, 3601.

[17] a) E. R. Draper, D. J. Adams, *Chem. Commun.* **2016**, *52*, 8196 – 8206; b) Z. Chen, Z. Lv, G. Qing, T. Sun, *J. Mater. Chem. B* **2017**, *5*, 3163 – 3171; c) Z. Wu, R. Xue, M. Xie, X. Wang, Z. Liu, M. Drechsler, J. Huang, Y. Yan, *J. Phys. Chem. Lett.* **2018**, *9*, 163 – 169.

[18] a) Z. Sun, Q. Huang, T. He, Z. Li, Y. Zhang, L. Yi, *ChemPhysChem* **2014**, *15*, 2421 – 2430; b) C. D. Jones, J. W. Steed, *Chem. Soc. Rev.* **2016**, *45*, 6546 – 6596.

[19] a) C. Wang, Q. Chen, F. Sun, D. Zhang, G. Zhang, Y. Huang, R. Zhao, D. Zhu, *J. Am. Chem. Soc.* **2010**, *132*, 3092 – 3096; b) Z.-X. Liu, Y. Feng, Z.-C. Yan, Y.-M. He, C.-Y. Liu, Q.-H. Fan, *Chem. Mater.* **2012**, *24*, 3751 – 3757; c) R. Yang, S. Peng, T. C. Hughes, *Soft Matter* **2014**, *10*, 2188 – 2196; d) X. Tan, Z. Li, M. Xia, X. Cheng, *RSC Adv.* **2016**, *6*, 20021 – 20026.

[20] K. K. Kartha, N. K. Allampally, A. T. Politi, D. D. Prabhu, H. Ouchi, R. Q. Albuquerque, S. Yagai, G. Fernández, *Chem. Sci.* **2019**, *10*, 752 – 760.

[21] M. M. J. Smulders, M. M. L. Nieuwenhuizen, T. F. A. de Greef, P. van der Schoot, A. P. H. J. Schenning, E. W. Meijer, *Chem. Eur. J.* **2010**, *16*, 362 – 367.

[22] K. K. Kartha, V. K. Praveen, S. S. Babu, C. Sandeep, A. Ajayaghosh, *Chem. Asian J.* **2015**, *10*, 2250 – 2256.

[23] J. S. Valera, J. Calbo, R. Gómez, E. Ortí, L. Sánchez, *Chem. Commun.* **2015**, *51*, 10142 – 10145.

[24] J. W. Fredy, A. Mendez-Ardoy, S. Kwangmettatam, D. Bochicchio, B. Matt, M. C. A. Stuart, J. Huskens, N. Katsonis, G. M. Pavan, T. Kudernac, *Proc. Natl. Acad. Sci. USA* **2017**, *114*, 11850 – 11855.

[25] T. Kobayashi, Y. Kitamoto, Y. Hirai, T. Kajitani, T. Seki, S. Yagai, *Commun. Chem.* **2018**, *1*, 58.